Volume 4
Number 7
July 2023
Pages 449–526

# RSC Chemical Biology

rsc.li/rsc-chembio

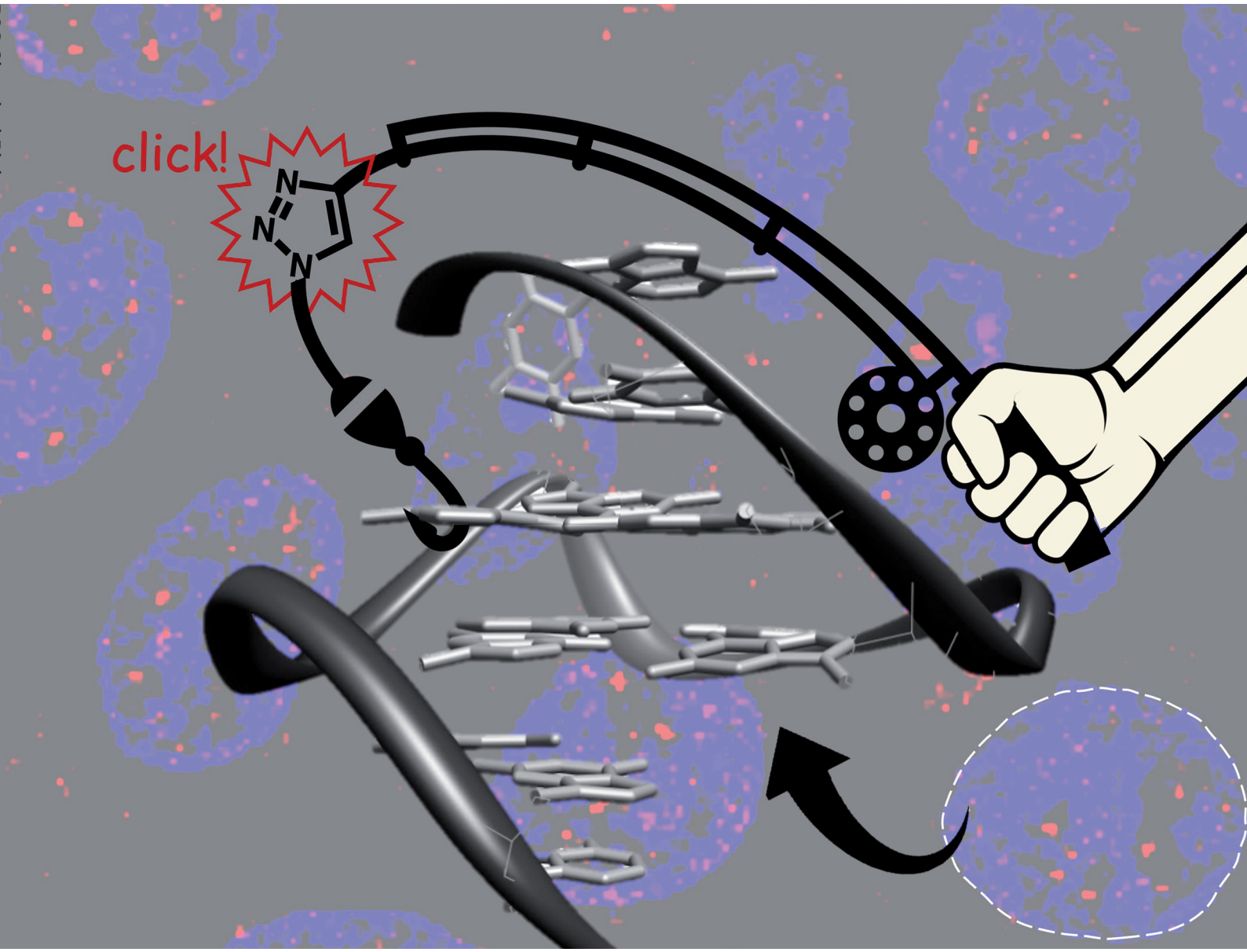


ISSN 2633-0679

ROYAL SOCIETY OF CHEMISTRY

**PAPER**
Ibai E. Valverde, David Monchaud *et al.*
The multivalent G-quadruplex (G4)-ligands MultiTASQs allow for versatile click chemistry-based investigations

RSC Chemical Biology

ROYAL SOCIETY OF CHEMISTRY

PAPER

View Article Online
View Journal | View Issue



Cite this: *RSC Chem. Biol.*, 2023, 4, 456

# The multivalent G-quadruplex (G4)-ligands MultiTASQs allow for versatile click chemistry-based investigations†

Francesco Rota Sperti, Jérémie Mitteaux, Joanna Zell, Angélique Pipier, Ibai E. Valverde * and David Monchaud *

Chemical biology hinges on multivalent molecular tools that can specifically interrogate and/or manipulate cellular circuitries from the inside. The success of many of these approaches relies on molecular tools that make it possible to visualize biological targets in cells and then isolate them for identification purposes. To this end, click chemistry has become in just a few years a vital tool in offering practically convenient solutions to address highly complicated biological questions. We report here on two clickable molecular tools, the biomimetic G-quadruplex (G4) ligands MultiTASQ and $^{az}$MultiTASQ, which benefit from the versatility of two types of bioorthogonal chemistry, CuAAC and SPAAC (the discovery of which was very recently awarded the Nobel Prize of chemistry). These two MultiTASQs are used here to both visualize G4s in and identify G4s from human cells. To this end, we developed click chemo-precipitation of G-quadruplexes (G4-click-CP) and *in situ* G4 click imaging protocols, which provide unique insights into G4 biology in a straightforward and reliable manner.

Received 23rd January 2023,
Accepted 12th May 2023

DOI: 10.1039/d3cb00009e

rsc.li/rsc-chembio



## I. Introduction

Click chemistry, either the copper(I)-catalyzed azide-alkyne cycloaddition (CuAAC) developed by Meldal[1] and Sharpless[2] or its metal-free counterpart strain-promoted azide-alkyne cycloaddition (SPAAC) developed by Bertozzi,[3] finds wide applications in chemistry and chemical biology, as recognized recently by the Nobel committee.[4] Many bioorthogonal strategies aiming at interrogating cell circuitries with molecular modulators now hinge on click chemistry: for example, click chemistry is widely used for imaging purposes[5] in both fixed (CuAAC) and live cells (SPAAC); it is also used for pulling down probes in interaction with their cellular partners and/or genomic targets followed by either proteomics ('click pull-down' or 'click-proteomics') or sequencing ('click-seq' or 'chem-click-seq'). An illustrative example is the clickable analog of Remodelin,[6] which was clicked *in situ* to AF488-azide for localization purposes in human osteosarcoma (U2OS) cells, and to a biotin-azide derivative to identify the acetyltransferase NAT10 as its cellular partner.[6] Similarly, a clickable analog of the BET inhibitor JQ1[7] termed JQ1-PA was labeled *in situ* with AF488-azide for localization purposes in human leukemia (MV4-11) cells, and to a biotin-azide derivative to identify the genomic binding sites of bromodomain-containing protein 4 (BRD4), which is targeted by JQ1.[8] Also, a series of clickable Olaparib[9] derivatives were exploited to confirm the specificity of this drug to poly(ADP-ribose)-polymerase 1 (PARP1) in human cervical cancer (HeLa) cells, *via* a combination of click-imaging and click-proteomics.[10]

In the field of G-quadruplexes (G4s), the CuAAC allowed first and foremost for the modular synthesis of a wide variety of G4-ligands.[11–13] When applied to bioorthogonal investigations, click chemistry has permitted the very first visualization of G4s in human cells, using a clickable pyridostatin (PDS)[14] derivative termed PDS-α labeled *in situ* with AF594-azide in U2OS (by CuAAC),[15] then in human colon cancer (HT-29) cells using clickable PhenDC3[16] derivatives (PhenDC3-alk for CuAAC and PhenDC3-az for SPAAC)[17] and again in U2OS with a clickable L2H2-6OTD[18] derivative termed L2H2-6OTD-az (by SPAAC).[19] Another approach referred to as G4-GIS (for G4-ligand guided immunofluorescence staining) involved a series of clickable pyridodicarboxamide (PDC) derivatives, notably PDC-4,3-Alk that was used either pre-clicked or *in situ* clicked with 5-BrdU-$N_3$ (a 5-bromo-2′-deoxyuridine functionalized with an azide group) in human lung cancer (A549) cells, prior to being immunodetected using an anti-5-BrdU antibody. Two proteomics-based approaches termed G4-LIMCAP (for G4 ligand-mediated cross-linking and

*ICMUB, CNRS UMR6302, Université de Bourgogne, 9 Avenue Alain Savary, 21078 Dijon, France. E-mail: ibai.valverde@u-bourgogne.fr, david.monchaud@cnrs.fr*

† Electronic supplementary information (ESI) available: Synthesis and characterization of MultiTASQ (Fig. S1–S5) and $^{az}$MultiTASQ (Fig. S6–S10); oligonucleotide preparation and used buffers (Table S1); additional results for FRET-melting experiments and pull-down assays (Fig. S11). See DOI: **https://doi.org/10.1039/d3cb00009e**

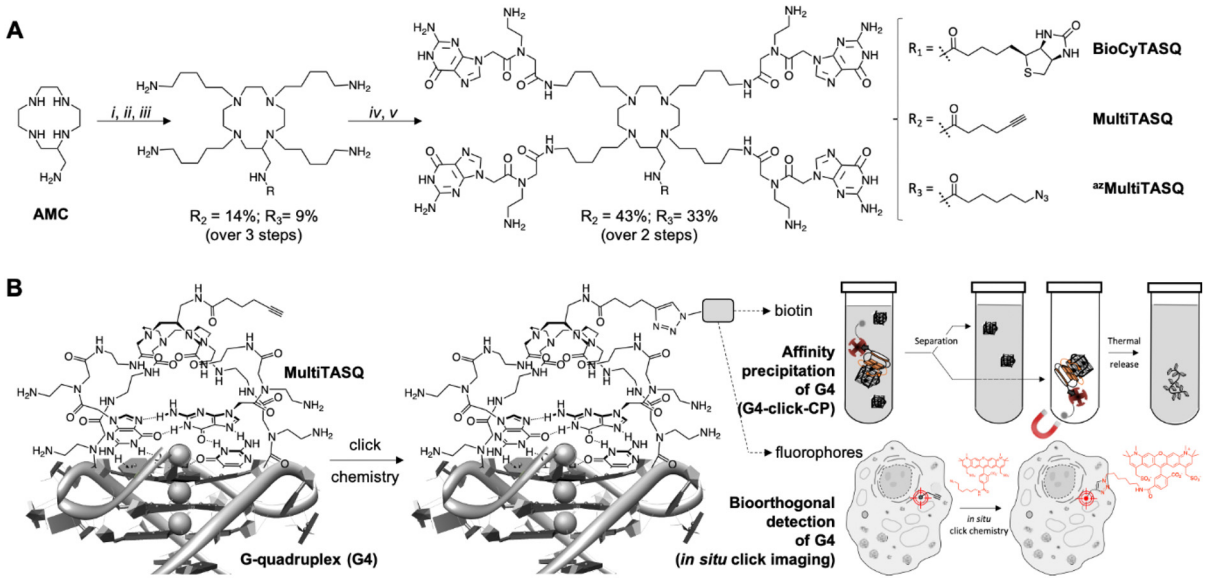


Fig. 1 (A) Chemical structure and synthesis of BioCyTASQ, MultiTASQ and $^{az}$MultiTASQ; (i) R-$CO_2$H, TSTU, DIPEA, DMF; (ii) MsO-$(CH_2)_5$-NHBoc, $K_2CO_3$, $CH_3CN$; (iii) TFA; (iv) Boc-$^{PNA}$G-OH, HBTU, DIPEA, DMF; (v) TFA. (B) Schematic representation of the G-quartet/G-quartet interaction between the TASQ and a DNA/RNA G4, and of the click chemistry-based investigations made possible with MultiTASQs, *i.e.*, G4 isolation by affinity capture (clicked biotin) and optical imaging (clicked fluorophore).

pull-down)[20] and co-binding-mediated protein profiling (CMPP),[21] based on two other clickable PDS derivatives (PDB-DA-A and photoPDS, respectively), were recently used to uncover several new G4-binding proteins in human breast cancer (MDA-MB-231) cells, immortalized human fibroblast (SV589) cells,[20] and human embryonic kidney (HEK293T) cells.[21]

These examples brightly illustrate the interest of clickable probes in chemical biology in general, and in the G4 field in particular. Following up on our recent use of biotinylated G4-specific molecular probes BioTASQ, BioCyTASQ and BioTriazo-TASQ (Fig. 1A)[22–26] to isolate G4s *via* affinity precipitation, we aim here at further exploiting the exquisite G4 selectivity of TASQs: this specificity originates in the biomimetic, like-likes-like interaction between the G-quartet of the G4 and the synthetic G-quartet of the TASQ (for the template-assembled synthetic G-quartet, Fig. 1B).[27,28] TASQs are smart ligands that adopt their G4-affinic conformation only in the presence of their G4 targets, which thus makes them uniquely actively selective for G4s. We thus report here on our new, patented MultiTASQ technology (Fig. 1A),[29] which comprises multivalent TASQs with either an alkyne appendage (MultiTASQ) for CuAAC applications or an azide chain (azidoMultiTASQ, or $^{az}$MultiTASQ) for SPAAC applications, used for both click chemo-precipitation of G-quadruplexes (G4-click-CP) and click-imaging purposes (Fig. 1B).

## II. Design and synthesis of MultiTASQs

The design of MultiTASQs was inspired by the recently developed biotinylated TASQs,[22–25] with the goal of adding a greater degree of bio-compatibility and versatility. By changing the biotin appendage for an alkyne or an azide one, the resulting TASQ could be usable for live-cell incubation as the triple bond/azide minimally divert TASQ biodistribution[5] (unlike biotin that can create H-bonds with various cellular components), which makes this technology implementable in living cells.[30] Furthermore, the inability of the alkyne/azide appendage to form a H-bond will also preclude internal poisoning of the TASQ, found to be responsible for the lower G4-affinity of BioTASQ as compared to non-biotinylated TASQ.[23,24]

The synthetic pathway of MultiTASQs (Fig. 1 and Fig. S1–S10, ESI†) thus started from the aminomethylcyclen (AMC)[31] coupled with 5-hexynoic acid (MultiTASQ) or 6-azido-hexanoic acid ($^{az}$MultiTASQ) to obtain the corresponding AMC derivatives in 38 and 21% chemical yield, respectively. These derivatives were subsequently reacted with an excess of 5-(Boc-amino)pentyl-mesylate linker (8.0 mol equiv., 38 and 40% chemical yield, respectively), deprotected by TFA (quantitative) and coupled to Boc-$^{PNA}$G-OH[32] (4.4 mol equiv.) to provide the Boc-protected MultiTASQs with 43 and 33% chemical yield, respectively. MultiTASQs were then deprotected prior to use with TFA, which led to the final compounds in a 6.2 and 2.7% chemical yield over 5 steps, respectively.

## III. *In vitro* validation of MultiTASQs

### G4 affinity and selectivity of MultiTASQs

The G4 affinity of the two MultiTASQs was evaluated *via* competitive FRET-melting assay[33] against two DNA G4s (Table 1), from sequences found in human telomere (F21T) and in the promoter region of the Myc gene (F-Myc-T), and two RNA G4s (Table 1), from sequences found in the human telomeric transcript (F-TERRA-T) and in the 5′-UTR region of the VEGF mRNA (F-VEGF-T). These experiments were performed with

Table 1 Oligonucleotides used in this study

| Oligonucleotides used in this study | | | |
|---|---|---|---|
| Status | Nature | Name | Sequence |
| FRET-melting assay | | | |
| Bi-labeled | DNA | F21T | FAM-d[$^{5'}$GGGTTAGGGTTAGGGTTAGGG$^{3'}$]-TAMRA |
| | | F-Myc-T | FAM-d[$^{5'}$GAGGGTGGGGAGGGTGGGGAAG$^{3'}$]-TAMRA |
| | | F-Kit2-T | FAM-[$^{5'}$CGGGCGGGCGCGAGGGAGGGG$^{3'}$]-TAMRA |
| | RNA | F-TERRA-T | FAM-r[$^{5'}$GGGUUAGGGUUAGGGUUAGGG$^{3'}$]-TAMRA |
| | | F-VEGF-T | FAM-r[$^{5'}$GGAGGAGGGGAGGAGGA$^{3'}$]-TAMRA |
| | | F-NRAS-T | FAM-[$^{5'}$GGGAGGGGCGGGUCUGGG$^{3'}$]-TAMRA |
| Fluorescence quenching assay | | | |
| Mono-labeled | DNA | $^{5'}$Cy5-Myc | Cy5-d[$^{5'}$GAGGGTGGGGAGGGTGGGGAAG$^{3'}$] |
| Fluorescence pull-down experiments | | | |
| Mono-labeled | DNA | F-22AG | FAM-d[$^{5'}$AGGGTTAGGGTTAGGGTTAGGG$^{3'}$] |
| | | F-Myc | FAM-d[$^{5'}$GAGGGTGGGGAGGGTGGGGAAG$^{3'}$] |
| | | F-duplex | FAM-d[$^{5'}$TATAGCTATATTTTTTTATAGCTATA$^{3'}$] |
| | RNA | F-TERRA | FAM-r[$^{5'}$GGGUUAGGGUUAGGGUUAGGG$^{3'}$] |
| | | F-VEGF | FAM-r[$^{5'}$GGAGGAGGGGAGGAGGA$^{3'}$] |
| | | F-NRAS | FAM-[$^{5'}$GGGAGGGGCGGGUCUGGG$^{3'}$] |
| Competitor for FRET-melting experiments | | | |
| Unlabeled | DNA | CT-DNA | Calf thymus DNA, ss- and ds-DNA, 42% GC-content (D1501) |
| qPCR pull-down experiments | | | |
| Unlabeled | DNA | G4-strand | d[$^{5'}$TAGC$_2$AT$_2$CAGC$_2$GTA$_2$CAG$_2$CAGTG$_2$A$_2$(GA)$_3$CAGA(CAG$_3$)$_4$(CAGTA)$_2$GA$_2$C$_2$TA$_2$TG$_2$TGT$_3$GATG$_2$TATCTA$_2$$^{3'}$] |
| | | Primer | G4-R1: d[$^{5'}$TTAGATACCATCAAACACCATTAGG$^{3'}$] |
| Primers for G4RP-RT-qPCR experiments | | | |
| Unlabeled | DNA | NRAS | Forward: d[$^{5'}$ATGACTGAGTACAAACTGGTGGT$^{3'}$] |
| | | | Reverse: d[$^{5'}$CATGTATTGGTCTCTCATGGCAC$^{3'}$] |
| | | VEGF | Forward: d[$^{5'}$CCTTGCCTTGCTGCTCTACC$^{3'}$] |
| | | | Reverse: d[$^{5'}$AGATGTCCACCAGGGTCTCG$^{3'}$] |

labeled DNA/RNA (0.2 μM) and TASQs (1 μM, 5 mol equiv.) in the absence or presence of an excess of competitive dsDNA (calf thymus DNA, or CT-DNA, 15 or 50 mol equiv.).

Results seen in Fig. 2A and Table 2 indicated that (i) TASQs display a lower affinity for DNA G4s (averaged $\Delta T_{1/2}$ = 3.9 and 4.3 °C for MultiTASQ and $^{az}$MultiTASQ, respectively, at 5 mol equiv. ligand) as compared to RNA G4s (averaged $\Delta T_{1/2}$ = 11.4 and 11.8 °C for MultiTASQ and $^{az}$MultiTASQ, respectively), and (ii) TASQs are extremely selective for G4s over dsDNA (averaged $^{FRET}S > 1.0$ for both TASQs at 50 mol equiv. CT-DNA). These results were in line with what was obtained with the previously reported TASQs.[24,25] Their ability to interact efficiently and selectively with G4 whatever their structure was further demonstrated by competitive FRET-melting experiments performed with an atypical G4[34] that folds from a sequence found in the promoter region of the Kit gene (Fig. S11, ESI†), with $\Delta T_{1/2} = 5.8 \pm 0.2$ and $7.7 \pm 1.0$; $^{FRET}S = 0.57$ and >1.0 for MultiTASQ and $^{az}$MultiTASQ, respectively.

Their G4-affinity was confirmed *via* an equilibrium-binding assay that relies on the use of a G4 labeled with a Cy5 dye (on its 5′-end) that is quenched upon ligand binding.[35] We used $^{5'}$Cy5-Myc here as it was initially validated as a G4 model for studying the interaction with established ligands such as TMPyP4 and PhenDC3. We calibrated this assay, termed fluorescence quenching assay (FQA), with PhenDC3 and obtained an affinity in the nanomolar range ($^{app}K_D$ = 57.7 ± 0.2 nM), as initially described. As seen in Fig. 2B and Table 2, the G4 affinity of MultiTASQs was found to be in the micromolar range ($^{app}K_D$ = 1.44 ± 0.1 and 0.90 ± 0.1 μM for MultiTASQ and $^{az}$MultiTASQ, respectively), in line with that of BioCyTASQ ($^{app}K_D$ = 1.01 ± 0.1 μM).

Collectively, the results obtained by both FRET-melting assay and FQA showed that the modification of the TASQs' appendage did not modify their affinity and selectivity for G4s. This is consistent with the interaction mode schematically represented in Fig. 1B, in which the TASQ interacts with its G4 target thanks to its intramolecular G-quartet and the appendage is located on the other side of the TASQ, being thus devoid of any G4 interaction.

### Click chemo-precipitation of G4s: the fluorescence-based protocol

G4-click-CP was performed with both clicked MultiTASQ and $^{az}$MultiTASQ (along with BioCyTASQ as a control) against the oligonucleotides used for FRET-melting assay with only the 5′-FAM label (*i.e.*, two DNA G4s: F-22AG and F-Myc, two RNA G4s: F-TERRA and F-VEGF, along with F-duplex as a control, Table 1). MultiTASQ was coupled with azide-PEG$_3$-biotin by CuAAC and $^{az}$MultiTASQ with dibenzocyclooctyne (DBCO)-PEG$_4$-biotin by SPAAC (Fig. 2C, and the ESI†). MultiTASQ was

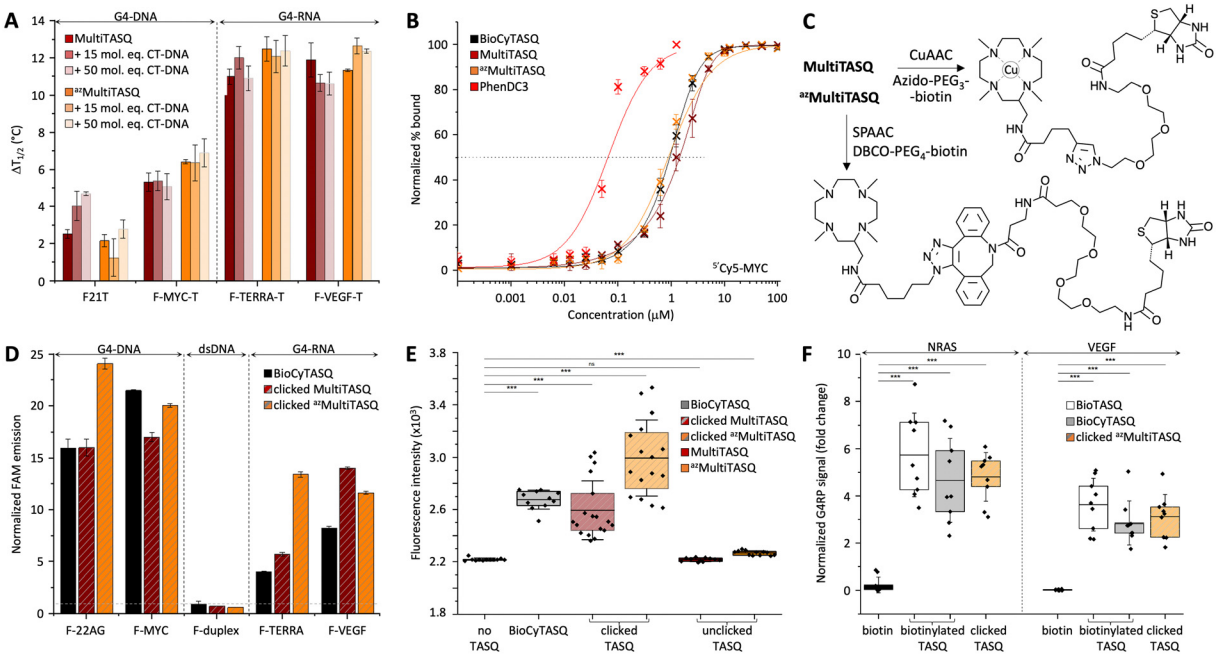


Fig. 2 (A) FRET-melting assay results ($\Delta T_{1/2}$, in °C) collected with doubly labeled G4s (0.2 μM; DNA: F-21-T, F-Myc-T; RNA: F-VEGF-T, F-TERRA-T) in the presence of MultiTASQs (1.0 μM) and increasing amounts of unlabeled duplex-DNA (calf thymus DNA, CT-DNA, 15 and 50 mol equiv.; $n > 2$). Of note, the increase in mid-transition temperatures observed in the presence of an excess of CT-DNA likely originates in an increase of the ionic strength of the solution upon addition of a large amount of $Na^+$-containing DNA competitor. (B) Ligands' binding to 5′ Cy5-Myc G4 (20 nM) monitored by Cy5 fluorescence quenching upon the addition of increasing amounts (1 pM to 100 μM) of TASQs (and PhenDC3 as control). (C) Schematic representation of biotinylation of TASQs by biorthogonal functionalization of MultiTASQ by CuAAC and azMultiTASQ by SPAAC. (D) Results of the *in vitro* G4 pull-down protocol ($n$ = 3) performed with FAM-labeled oligonucleotides (1.0 μM; DNA: F-22AG, F-Myc; RNA: F-TERRA, F-VEGF; the hairpin F-duplex as control) and clicked MultiTASQs (BioCyTASQ as control) quantified by the increase in fluorescence during the elution step, normalized to the control (without TASQ). (E) qPCR pull-down results (SYBR green fluorescence intensity; $n$ = 3) for experiments performed with a 97-nt G4-containing DNA sequence (4 μM) without TASQ (control), with clicked MultiTASQs (40 μM, BioCyTASQ as control) or unclicked MultiTASQs (40 μM, control). (F) G4RP signals of biotin (control) *versus* clicked MultiTASQ (BioTASQ and BioCyTASQ as controls) *via* RT-qPCR quantification of NRAS and VEGFA mRNA levels in MCF7 ($n$ = 3). *$p < 0.05$, **$p < 0.01$, ***$p < 0.001$.

clicked to azide-$PEG_3$-biotin in the presence of an excess (2.5 mol equiv.) of copper to take into account the copper chelation by the central cyclen template. The click mixture was prepared in water by mixing $(MeCN)_4Cu{\cdot}BF_4$ with THPTA ((tris(3-hydroxypropyltriazolylmethyl)amine) before the addition of sodium ascorbate; MultiTASQ was separately mixed with a slight excess or azido-$PEG_4$-biotin (1.1 mol equiv.) in a 1 : 1 mixture of water and 1-butanol (1 : 1). The two solutions were then mixed and stirred at 25 °C for 1 h (an HPLC-MS monitoring allowed for assessing the efficiency of the CuAAC, if needed). Of note: (i) the final proportion of 1-butanol is 2% only, which is compatible with the stability of G4s in the condition of the experiments; and (ii) the demetallation of clicked MultiTASQ, usually performed with $Na_2S$ treatment,[25,36] is avoided here for a reproducibility issue related to the loss of material during the precipitation step (the presence of copper within the cyclene template did not affect the properties of the TASQ, Fig. S11, ESI†). azMultiTASQ was mixed with a slight excess of DBCO-$PEG_4$-biotin conjugate (1.1 mol equiv.) in water and stirred for 1 h at 37 °C (again, an HPLC-MS monitoring allowed for assessing the efficiency of the SPAAC, if needed). Of note: in both instances, we performed affinity control experiments (FRET-melting) that showed that the biotinylation of TASQs by click chemistry does not affect their G4-interacting properties (Fig. S11, ESI†).

The clicked TASQs (10 μM) were then mixed with nucleic acids (1 μM) and streptavidin-coated magnetic beads for 1 h at 25 °C before the isolation of the DNA (or RNA)/TASQ/beads complexes by magnetic immobilization and release of captured DNA (or RNA) by a thermal denaturation step (8 min at 90 °C). The efficiency of the capture was quantified by the FAM emission calculated after the denaturation step, expressed as fold enrichment after normalization to the control experiment performed without TASQ. As seen in Fig. 2D and Table 2, the three TASQs were found to capture G4s with a similar efficiency; however, contrarily to FRET-melting results, their performance was better with G4-DNA (averaged enrichment = 16.5- and 22.0-fold for clicked MultiTASQ and azMultiTASQ, respectively) than with G4-RNA (averaged enrichment = 9.8- and 12.5-fold for clicked MultiTASQ and azMultiTASQ, respectively). These results were in line with those of BioCyTASQ (averaged enrichment = 18.7- and 6.1-fold for DNA and RNA G4s, respectively) and BioTriazoTASQ.[25] This trend is not easily rationalized but likely originates in the difference of both the experimental setup between FRET-melting and pull-down experiments (variable-temperature *versus* isothermal experiments) and, most importantly, the effect monitored (thermal stabilization *versus* affinity precipitation). We can postulate that the almost exclusively parallel topology of RNA G4s enables a more

Table 2 Summary of the *in vitro* results collected in this study

| | FRET-melting assay | | | |
|---|---|---|---|---|
| | F21T | F-Myc-T | F-TERRA-T | F-VEGF-T |
| MultiTASQ | 2.5 ± 0.2 °C<br>$CT_{(15eq.)}$: 4.4 ± 0.8 °C<br>$^{FRET}S$ = 1.7<br>$CT_{(50eq.)}$: 4.7 ± 0.1 °C<br>$^{FRET}S$ = 1.8 | 5.3 ± 0.3 °C<br>$CT_{(15eq.)}$: 5.4 ± 0.5 °C<br>$^{FRET}S$ = 1.0<br>$CT_{(50eq.)}$: 5.1 ± 0.7 °C<br>$^{FRET}S$ = 0.9 | 11.0 ± 0.9 °C<br>$CT_{(15eq.)}$: 12.0 ± 0.6 °C<br>$^{FRET}S$ = 1.1<br>$CT_{(50eq.)}$: 10.9 ± 0.7 °C<br>$^{FRET}S$ = 1.0 | 11.9 ± 0.4 °C<br>$CT_{(15eq.)}$: 10.7 ± 0.4 °C<br>$^{FRET}S$ = 0.9<br>$CT_{(50eq.)}$: 10.6 ± 0.6 °C<br>$^{FRET}S$ = 0.9 |
| $^{az}$MultiTASQ | 2.2 ± 0.3 °C<br>$CT_{(15eq.)}$: 1.3 ± 0.9 °C<br>$^{FRET}S$ = 0.6<br>$CT_{(50eq.)}$: 2.8 ± 0.8 °C<br>$^{FRET}S$ = 1.3 | 6.4 ± 0.2 °C<br>$CT_{(15eq.)}$: 6.3 ± 0.9 °C<br>$^{FRET}S$ = 1.0<br>$CT_{(50eq.)}$: 6.9 ± 0.5 °C<br>$^{FRET}S$ = 1.1 | 12.4 ± 0.6 °C<br>$CT_{(15eq.)}$: 12.1 ± 0.9 °C<br>$^{FRET}S$ = 0.9<br>$CT_{(50eq.)}$: 12.4 ± 0.8 °C<br>$^{FRET}S$ = 1.0 | 11.3 ± 0.4 °C<br>$CT_{(15eq.)}$: 12.6 ± 0.4 °C<br>$^{FRET}S$ = 1.1<br>$CT_{(50eq.)}$: 12.4 ± 0.1 °C<br>$^{FRET}S$ = 1.1 |

| | Fluorescence quenching assay | | | |
|---|---|---|---|---|
| | PhenDC3 | BioCyTASQ | MultiTASQ | $^{az}$MultiTASQ |
| $^{5'}$Cy5-Myc | 57.7 ± 0.2 nM | 1.01 ± 0.1 μM | 1.44 ± 0.1 μM | 0.90 ± 0.1 μM |

| | Fluorescence pull-down experiments | | | | |
|---|---|---|---|---|---|
| | F-22AG | F-Myc | F-duplex | F-TERRA | F-VEGF |
| BioCyTASQ | 15.9 ± 0.9-fold | 21.5 ± 0.1-fold | 0.9 ± 0.2-fold | 4.0 ± 0.0-fold | 8.2 ± 0.2-fold |
| Clicked MultiTASQ | 16.0 ± 0.8-fold | 17.0 ± 0.4-fold | 0.7 ± 0.0-fold | 5.7 ± 0.2-fold | 14.0 ± 0.1-fold |
| Clicked $^{az}$MultiTASQ | 24.1 ± 0.5-fold | 20.0 ± 0.2-fold | 0.6 ± 0.1-fold | 13.4 ± 0.3-fold | 11.6 ± 0.2-fold |

| | qPCR pull-down experiments | | | | | |
|---|---|---|---|---|---|---|
| | No TASQ | BioCyTASQ | MultiTASQ | Clicked MultiTASQ | $^{az}$MultiTASQ | Clicked $^{az}$MultiTASQ |
| 97-nt ODN | 2218 | 2675 ± 73<br>ΔFI = 457 | 2215 ± 13<br>ΔFI = −3 | 2594 ± 225<br>ΔFI = 376 | 2266 ± 18<br>ΔFI = 48 | 2924 ± 291<br>ΔFI = 706 |

| | G4RP RT-qPCR | | | |
|---|---|---|---|---|
| | Biotin | BioTASQ | BioCyTASQ | Clicked $^{az}$MultiTASQ |
| NRAS | 0.2 ± 0.3-fold | 5.7 ± 1.7-fold | 4.6 ± 1.8-fold | 4.8 ± 1.0-fold |
| VEGF | 0.1 ± 0.1-fold | 3.6 ± 1.1-fold | 2.8 ± 0.9-fold | 3.1 ± 0.9-fold |

straightforward interaction with the TASQs (better G-quartet accessibility), which leads to better G4 stabilization. Conversely, we can postulate that the richer topological diversity of DNA G4s offers secondary binding interactions (loops) which make the TASQ/G4 complex stronger, and thus, more efficiently captured and isolated by precipitation. These hypotheses are appealing but remain speculative at present, without more accurate structural information. However, these results were interesting as none of the TASQs were able to pull dsDNA down (between 0.6 and 0.9-fold enrichment with F-duplex), confirming the excellent G4-selectivity of TASQs.

### Click chemo-precipitation of G4s: the qPCR-based protocol

It was thus of interest to assess the G4-capturing ability of TASQ in more biologically relevant conditions. To this end, we included a G4-forming sequence in a 97-nucleotide long DNA strand (97-nt ODN, Table 1), devoid of fluorescent tags, which makes its detection possible only through qPCR analyses.[37,38] G4-click-CP was here performed without TASQ (control), with both MultiTASQ and $^{az}$MultiTASQ (10 μM) either unclicked (controls) or clicked to biotin derivatives, along with BioCyTASQ. As above, MultiTASQ was coupled with azide-$PEG_3$-biotin by CuAAC (or not) and $^{az}$MultiTASQ with DBCO-$PEG_4$-biotin by SPAAC (or not), and incubation of the G4-containing DNA strand (1 μM) in the presence of the streptavidin-coated magnetic beads for 2 h at 25 °C. After isolation of the DNA/TASQ/bead complexes by magnetic immobilization, the captured DNA was released by a thermal denaturation step (8 min at 90 °C) and quantified through qPCR amplification (expressed as SYBR Green fluorescence intensity, FI). As seen in Fig. 2E and Table 2, no fluorescence increase was observed for the controls (FI = 2215 ± 13 and 2266 ± 18 with unclicked TASQs *versus* 2218 without TASQ; ΔFI = −3 and 48, respectively), thus confirming the need for a biotin bait for isolating G4s. Both clicked MultiTASQ and $^{az}$MultiTASQ efficiently pulled G4 down (FI = 2594 ± 225 and 2924 ± 291, respectively; ΔFI = 376 and 706), in a manner that is reminiscent to what is observed with BioCyTASQ (FI = 2675 ± 73; ΔFI = 457). These results thus confirmed that of the fluorescence-based G4-click-CP.

## IV. Cell-based applications of MultiTASQs

### G4RP protocol with clicked $^{az}$MultiTASQ

The two aforementioned G4-click-CP protocols were purely *in vitro* manipulations. To go a step towards using TASQ baits

under more relevant conditions, we considered both the G4RP protocol and *in situ* click imaging. We used $^{az}$MultiTASQ for the former and MultiTASQ for the latter.

The G4-RNA precipitation (G4RP) protocol was developed to detect folded G4s *in vivo*.[22,23,26] G4RP hinges on the cross-linking of naturally occurring G4s in living cells using formaldehyde prior to isolating them from cell lysates by affinity precipitation with BioTASQ. The G4RP protocol was validated by RT-qPCR analysis against well-established G4-containing transcripts including VEGF (see above) and a sequence found in the 5′-UTR region of the NRAS mRNA. To date, the G4RP-RT-qPCR protocol was performed with BioTASQ only;[22,23,26] we thus decided to evaluate the properties of BioCyTASQ and a clicked $^{az}$MultiTASQ and to compare them with the initially used TASQ bait.

The interaction between TASQ and VEGF has already been investigated above; we thus checked their binding to NRAS by FRET-melting, performing the experiments with F-NRAS-T (0.2 μM) and TASQs (1 μM, 5 mol equiv.) in the absence or presence of an excess of competitive CT-DNA (15 or 50 mol equiv.). The results seen in Fig. S11A (ESI†) indicated that NRAS is efficiently stabilized by the TASQs with $\Delta T_{1/2}$ = 11.8 ± 0.7 and 14.6 ± 1.1 °C for MultiTASQ, $^{az}$MultiTASQ, respectively, with an exquisite selectivity ($^{FRET}S > 0.9$). We then checked that clicked TASQs efficiently pulled F-NRAS down *via* fluorescence G4-click-CP: the enrichment seen in Fig. S11B (ESI†) (5.5 ± 0.8 and 2.4 ± 0.3 for clicked MultiTASQ and $^{az}$MultiTASQ, respectively, *versus* 5.2 ± 0.9 for BioCyTASQ) confirmed that TASQs are indeed valuable baits for isolating this transcript *in vitro*.

The G4RP results depicted in Fig. 2F and Table 2 confirmed that the sterically demanding DBCO-based linker (comprising 1 triazole, 2 phenyls and 1 azacyclooctane, Fig. 2C) of clicked $^{az}$MultiTASQ does not hamper appropriate interaction with G4s *in vivo*. Indeed, MCF7 cells were trypsinyzed and then cross-linked with formaldehyde for 5 min prior to being resuspended in G4RP buffer and lysed (mechanical disruption). The lysate was then incubated with biotinylated BioTASQ and BioCyTASQ or the pre-clicked $^{az}$MultiTASQ (along with biotin as the control, 100 μM) in the presence of magnetic beads for 2 h at 4 °C. The beads were then isolated (magnetic immobilization), washed with G4RP buffer and subjected to thermal treatment (70 °C for 2 h) to both reverse the cross-link and free the captured nucleic acids. RNA fragments were isolated thanks to TRIZOL extraction and the quantity of NRAS and VEGF transcripts assessed by RT-qPCR. Under these conditions, clicked $^{az}$MultiTASQ efficiently enriched both NRAS and VEGF transcripts (enrichment = 4.8 ± 1.0 and 3.1 ± 0.9, respectively), less efficiently than BioTASQ (5.7 ± 1.7 and 3.6 ± 1.1, respectively) but with a better reproducibility, and more efficiently than BioCyTASQ (4.6 ± 1.8 and 2.8 ± 0.9, respectively). When compared to the biotin control (enrichment = 0.2 ± 0.3 and 0.02 ± 0.02, respectively), the two mRNA transcripts are enriched *ca.* >20 and >100-fold by the TASQs.

### Click imaging with MultiTASQ

To further exploit the versatility of MultiTASQs, we used their clickable handle to image G4 landscapes by clicking TASQs *in situ*, once in their cellular G4 sites, with fluorescent partners. This approach is different from the pre-targeted G4 imaging we previously reported on,[24,25] as the very nature of the clickable appendages of MultiTASQs (small size, no H-bonding ability) ensures that the target engagement of TASQs in cells is not biased, as it could be the case with the biotin appendage. To this end, we adapted the *in situ* click imaging protocol initially developed with PDS-α:[15] MCF7 human breast cancer cells were incubated either live (10 μM, 24 h) or after fixation (20 μM, 1 h) with MultiTASQ (to demonstrate the modularity of this approach). Bioorthogonal click reactions were then performed in cells with either AF488-azide or AF594-azide (to further demonstrate its modularity) by CuAAC. Of note, the *in situ* click reactions were always performed after cell fixation, in order to alleviate any issues relating to the possible cytotoxicity of the click mixture. Nuclei were subsequently stained with DAPI and images were collected by confocal laser scanning microscopy. The pattern seen in Fig. 3 corresponds to what has been described for the twice-as-smart probe N-TASQ (direct labeling)[39,40] and biotinylated TASQ (pre-targeted imaging):[24,25]

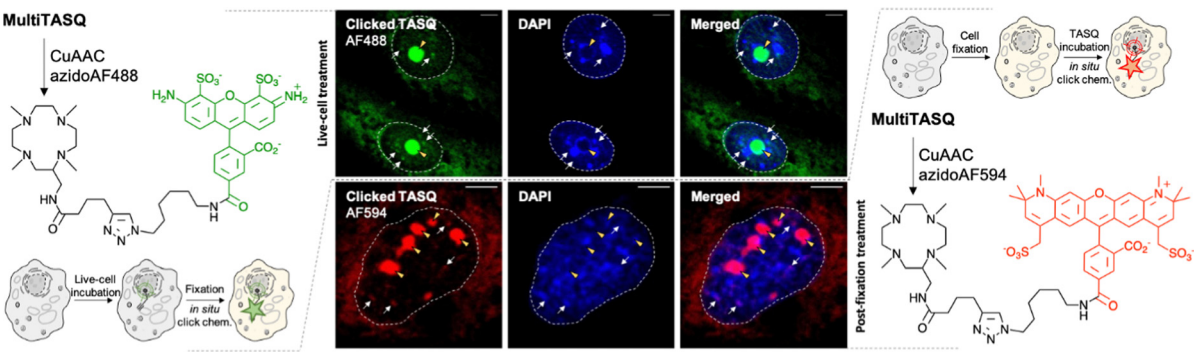


Fig. 3 Schematic representation of *in situ* click imaging protocols performed with MultiTASQ and either AF488-azide (left) or AF594-azide (right). Central panel: representative confocal images of MCF7 cells collected through DAPI (<425 nm) and GFP (500–550 nm) or TexasRed (>580 nm) filters. Cells are either treated live with MultiTASQ (10 μM, 24 h) prior to be fixed (upper panel) or fixed prior to being treated with MultiTASQ (20 μM, 1 h) (lower panel) and then subjected to Cu-catalyzed bioorthogonal labeling with either AF488-azide (upper panel) or AF594-azide (lower panel). Yellow arrows indicate nucleoli; white arrows indicated clicked MultiTASQ accumulation sites, ascribed to G4 *foci*; dashed lines delineate cell nuclei.

a dense nucleolar staining (yellow arrow) along with smaller, discrete nucleoplasmic *foci* (white arrow) ascribed to G4 clusters that fold during DNA transactions as they localize where DNA is at work (no DAPI staining). This approach, though qualitative in nature, provides high-quality images (high brightness, signal-to-noise ratio and *foci* definition) that are currently being exploited to assess whether and how G4-interacting agents (stabilizers[41] or destabilizers)[38,42] modulate G4 landscapes in cells. These results will be reported in due course.

# V. Conclusions

In conclusion, the design of MultiTASQs makes them benefit from the very high versatility and wide scope of click chemistry. The presence of azide/alkyne appendages offers more experimental opportunities than the biotinylated TASQs can offer as these appendages do not create unwarranted interactions (i) within the structure of the TASQ itself (avoiding internal structural poisoning), and (ii) with cellular components (preventing ligand dispersal), both mainly occurring *via* H-bond formation. Because both the biological activity and the target engagement of the TASQs are not biased, reliable live-cell experiments are possible.

We applied here in the G4 field only a minor fraction of the many possibilities offered by click chemistry.[43,44] However, the applications we developed with the clickable TASQs say much about how likely they are to become important companions for deciphering G4 biology. First, the click chemo-precipitation of G4s (G4-click-CP) helps assess whether suspected G4-forming sequences (both DNA and RNA) do actually fold into G4 structures in cells (G4RP[22] and G4DP[45] protocols, respectively). It also helps determine the extent to which G4 landscapes are modulated in cells by external effectors (*e.g.*, ligands) in a quantitative manner. The modularity of these protocols, which are implementable in either a targeted (RT-qPCR analysis) or genome-wide manner (sequencing), makes them fully complementary to existing methods including G4-seq[46] using the G4 ligand PDS,[14] or G4 ChIP-seq,[47] BG4-ChIP-seq,[48] G4P ChIP-seq[49] and G4 CUT&Tag[50,51] using the G4-specific antibody BG4[52] (CUT&Tag was also developed with the nanobody SG4)[53] for DNA G4s, and rG4-seq[54,55] using PDS, or BG4-RNA-IP[56] and rG4IP[57] using BG4 for RNA G4s, which altogether constitute a unique array of techniques to accurately portray G4 biology. Second, the *in situ* click imaging of G4s provides a more qualitative but also straightforward way to track G4s in cells. This fluorescence microscopy technique does not provide fine details about the sequences involved but a unique and dynamic visualization of the cellular G4 sites, which could be amenable to mechanistic interpretation *via* both colocalization studies (with organelle markers, DNA damage markers, *etc.*) and longitudinal studies (*e.g.*, upon ligand treatment). Optical imaging techniques aiming at tracking G4 which can also be more quantitative in nature and implementable as high-throughput screens such as the flow cytometry-based protocol BG-flow,[58] based on the BG4, used to discriminate between cell status and monitor ligand-mediated modulations of G4 signatures.

Clickable TASQs thus allow for the implementation of protocols that represent two faces only of a panel of techniques devoted to uncovering the finest details of G4 biology. With this growing portfolio of tools in hands, new experimental, strategic and mechanistic opportunities are now available for pushing the G4 field ever further.

# VI. Material and methods

## 1. Chemistry & oligonucleotides

The synthesis and chemical characterization of MultiTASQ and $^{az}$MultiTASQ are described in the ESI;† the oligonucleotides used in this study along with the preparation of their higher-order structures are also described in the ESI.† The click protocols are the following:

**1a. CuAAC.** 5 μL of a 1 M solution (DMSO) of $(MeCN)_4Cu\cdot PF_6$ in DMSO were mixed with 7 μL of a 1 M solution ($H_2O$) of THPTA (tris(3-hydroxypropyltriazolylmethyl)amine), the mixture rapidly turned to a dark blue solution (Cu(II) salt). To this solution were added 10 μL of 1 M solution ($H_2O$) of sodium ascorbate to provide a colorless solution of Cu(I) salt. Separately, 20 μL of a 5 mM solution (water/1-butanol 1 : 1) of MultiTASQ were mixed with 1.1 μL of a 100 mM solution ($H_2O$) of azido-$PEG_4$-biotin conjugate, to which 4 μL of the aforementioned Cu(I) solution were added. The reaction was stirred for 1 h at 25 °C (HPLC-MS monitoring) and the stirring was stopped for a blue precipitate to form (Cu(II) salt). After centrifugation, the supernatant was removed and the clicked MultiTASQ used without further purification.

**1b. SPAAC.** 20 μL of a 1 mM solution ($H_2O$) of $^{az}$MultiTASQ were mixed with 2.2 μL of a 10 mM solution ($H_2O$) of dibenzocyclooctyne-$PEG_4$-biotin conjugate (DBCO-$PEG_4$-biotin). The reaction was stirred for 1 h at 37 °C for 1 h (HPLC-MS monitoring) after which the clicked $^{az}$MultiTASQ was used without further purification.

## 2. Affinity measurements

**2a. FRET-melting assay.** FRET-melting experiments were performed in a 96-well format using a Mx3005P qPCR machine (Agilent) equipped with FAM filters ($\lambda_{ex}$ = 492 nm; $\lambda_{em}$ = 516 nm) in 100 μL (final volume) of CacoK10 (Table S1, ESI†) for F21T or CacoK1 (Table S1, ESI†) for F-Myc-T, F-Terra-T and F-VEGF-T, with 0.2 μM of labeled oligonucleotide (Table 1) and 1 μM of TASQ. Competitive experiments were performed with labeled oligonucleotide (0.2 μM), 1 μM TASQ and either 15 (3 μM) or 50 mol equiv. (10 μM) of the unlabeled competitor calf thymus DNA (CT-DNA). After an initial equilibration step (25 °C, 30 s), a stepwise increase of 1 °C every 30 s for 65 cycles to reach 90 °C was performed, and measurements were made after each cycle. Final data were analyzed with Excel (Microsoft Corp.) and OriginPro®9.1 (OriginLab Corp.). The emission of FAM was normalized (0 to 1), and $T_{1/2}$ was defined as the

 

temperature for which the normalized emission is 0.5; $\Delta T_{1/2}$ values are means of 3 triplicates.

**2b. Apparent $K_D$ measurement.** To a solution of $^{5'}$Cy5-myc (20 nM, Table 1) in 50 mM TrisHCl/Triton buffer (Table S1, ESI†) was added various concentrations (from 100 μM to 1 pM) of TASQs (and PhenDC3 as control). After mixing the solutions for 1 h at 25 °C, the fluorescence was measured using a ClarioStar® machine (BMG Labtech) equipped with a Cy5 filter ($\lambda_{ex}$ = 610 nm; $\lambda_{em}$ = 675 nm). Data were analyzed with Excel (Microsoft Corp.) and OriginPro®9.1 (OriginLab Corp.); the values were normalized ranging from 0 to 100, and the percentage of ligand bound was calculated subtracting the normalized values to 100. Three biological triplicates ($n$ = 3) were used.

## 3. G4-click-CP

**3a. Fluorescence pull-down assay.** The streptavidin MagneSphere® beads (Promega) were washed 3 times with 20 mM TrisHCl/$MgCl_2$ buffer (Table S1, ESI†). TASQs (10 μM) was mixed with 5′-labeled oligonucleotides (F-ON, 1 μM: F-22AG, F-Myc, F-duplex, F-TERRA and F-VEGF, Table 1, ESI†), MagneSphere® beads (32 μg) in the same TrisHCl buffer (320 μL final volume) and stirred for 1 h at 25 °C. The beads were immobilized (fast centrifugation (<2 s), magnet) and the supernatant removed. The solid residue was resuspended in 320 μL of TBS 1× buffer, heated for 8 min at 90 °C (gentle stirring 800 rpm) and then centrifuged for 2 min at 8900 rpm. The supernatant was taken up for analysis (magnet immobilization), after being distributed in 3 wells (100 μL each) of a 96-well plate, using a ClarioStar® machine (BMG Labtech) equipped with FAM filters ($\lambda_{ex}$ = 492 nm; $\lambda_{em}$ = 516 nm). Data were analyzed with Excel (Microsoft Corp.) and OriginPro®9.1 (OriginLab Corp.); normalized FAM emission values are means of 3 triplicates; each analysis comprises: (a) 3 control wells with F-ON and beads only (in order to quantify the non-specific F-ON/bead binding, the FAM emission of the solution was normalized to 1); and (b) 3 wells comprising solutions that resulted from experiments performed with F-ON, TASQ and beads (in order to quantify the capture capability of TASQ when compared to the control experiments).

**3b. qPCR pull-down assay.** The pull-down experiments were performed as above (*cf.* 3a), with the following modifications: (a) the oligonucleotide used was changed for a 97-nt ODN (Table 1) described in Jamroskovic *et al.*[37] and adapted in Mitteaux *et al.*[38] at the center of which the G4-forming sequence d[$(GGGCA)_4$] is included; (b) the buffer was replaced by the G4RP buffer (Table S1, ESI†); (c) the incubation time was changed for 2 h at 25 °C; (d) the output was changed for qPCR analyses: polymerase reactions were carried out in triplicate in a 96-well format using a Mx3005P qPCR machine (Agilent) equipped with FAM filters ($\lambda_{ex}$ = 492 nm; $\lambda_{em}$ = 516 nm) in 20 μL (final volume) of G4-1R primer (1 μL, 300 nM, Table 1), TASQ/ODN mixture (3.7 μL) in 10 μL iTaq™ Universal SYBR® Green Supermix (Bio-Rad) + KCl (5.3 μL, 100 mM). After a first denaturation step (95 °C, 5 min), a two-step qPCR comprising a denaturation step (85 °C, 10 s) and a hybridization/elongation step (60 °C, 15 s) for 33 cycles was performed, and measurements were made after each cycle. Final data were analyzed with OriginPro®9.1 (OriginLab Corp.). The starting emission (1st qPCR cycle) of SYBR Green (FI) was set to 2200 and the FI at the 33th cycle was used for calculation. Three biological triplicates ($n$ = 3) were used.

## 4. Cell-based investigations

**4a. G4RP-RT-qPCR protocol.** MCF7 cells (ECACC; Merck, Ref. 86012803) were seeded at 7 × $10^6$ cells per 175 $cm^2$ flask. After overnight adhesion, the medium was changed and cells were further cultured for 48 h before being trypsinized and then crosslinked using 1% (w/v) formaldehyde in fixing buffer (Table S1, ESI†) for 5 min at 25 °C. The crosslink was then quenched with 0.125 M glycine for 5 min, washed and rinsed (with DEPC-PBS, Table S1, ESI†). Cells were resuspended in G4RP buffer + 0.1% (w/v) SDS and then manually disrupted (syringe). After centrifugation (13 200 rpm, 10 min), the collected lysates (5% of which were collected as the input control) were incubated with 80 μM TASQs (or 80 μM biotin as control) and 90 μg of MagneSphere® beads (Promega) for 2 h at 4 °C. Magnetic beads were then washed (5 min, twice), before being resuspended in DEPC-PBS buffer supplemented with 0.4 U RNAse OUT. The beads were then incubated at 70 °C for 2 h to release captured G4-forming targets from the beads as unfolded. TRIZOL (1 mL) was then used to extract the RNA (using the manufacturer's instructions) and cleaned with RNA clean-up protocol (using the manufacturer's instructions) at 25 °C. The primer sets used for RT-qPCR are NRAS-forward and NRAS-reverse, and VEGF-forward and VEGF-reverse (Table 1). Extracted RNA was reverse transcribed with Superscript III (Invitrogen™ 18080-044) and random hexamer primers (Invitrogen™ N8080127) using the manufacturer's protocol to generate cDNA. cDNAs were quantified for target mRNAs using iTaq™ Universal 2X SYBR® Green Supermix (Bio-Rad) and specific primer sets with three technical replicates in each assay. $C(t)$ values of pull-down samples were normalized to the input control. Three biological replicates were used for all RT-qPCR-based quantifications. The final data were analyzed with Excel (Microsoft Corp.) and OriginPro®9.1 (OriginLab Corp.). For statistical hypothesis student's $t$-test and Welch's unequal variances $t$-test were used depending on variances equality.

**4b. *In situ* click imaging.** MCF7 cells were seeded on glass coverslips in a 24 well-plate for 24 h at 37 °C. Cells were either treated live with MultiTASQ (10 μM in DMEM, 24 h) then fixed (ice cold methanol, 10 min), or fixed and treated with MultiTASQ (20 μM in PBS, 1 h). Coverslips were washed with PBS (5 min, thrice), and click staining performed with AF488- or AF594-azide (1 μM) in PBS containing 0.05% IGEPAL CA-630, 1 mM $CuSO_4$ and 10 mM sodium ascorbate for 30 min, washed with PBS + 0.1% Triton (5 min, thrice), incubated with DAPI (10 min, 1 μg $mL^{-1}$ in PBS) and mounted with Fluoromount. Confocal imaging was performed using a confocal laser-scanning microscope (Leica TCS SP8) with a 63× objective lens and LASX software (Leica Microsystems CMS GmbH). Image processing was carried out using ImageJ.

## Conflicts of interest

The CNRS has licensed BioCyTASQ and MultiTASQs to Merck KGaA for commercialization.

## Acknowledgements

This work was supported by the CNRS (I. E. V. and D. M.), iSITE BFC (COMUE UBFC, PIA2, grant no. UB21018.MUB.IS, for D. M.), and the European Union (PO FEDER-FSE Bourgogne 2014/2020 programs, grant no. BG0021532 for D. M.). We also thank C. Deulvot & E. Noirot, DImaCell, AgroSup Dijon, INRAe, UBFC Dijon for technical assistance regarding confocal microscopy.

## References

1 C. W. Tornøe, C. Christensen and M. Meldal, *J. Org. Chem.*, 2002, **67**, 3057–3064.
2 V. V. Rostovtsev, L. G. Green, V. V. Fokin and K. B. Sharpless, *Angew. Chem., Int. Ed.*, 2002, **41**, 2596–2599.
3 N. J. Agard, J. A. Prescher and C. R. Bertozzi, *J. Am. Chem. Soc.*, 2004, **126**, 15046–15047.
4 D. Castelvecchi and H. Ledford, *Nature*, 2022, **610**, 242–243.
5 T. Cañeque, S. Müller and R. Rodriguez, *Nat. Rev. Chem.*, 2018, **2**, 202–215.
6 D. Larrieu, S. Britton, M. Demir, R. Rodriguez and S. P. Jackson, *Science*, 2014, **344**, 527–532.
7 P. Filippakopoulos, J. Qi, S. Picaud, Y. Shen, W. B. Smith, O. Fedorov, E. M. Morse, T. Keates, T. T. Hickman, I. Felletar, M. Philpott, S. Munro, M. R. McKeown, Y. Wang, A. L. Christie, N. West, M. J. Cameron, B. Schwartz, T. D. Heightman, N. La Thangue, C. A. French, O. Wiest, A. L. Kung, S. Knapp and J. E. Bradner, *Nature*, 2010, **468**, 1067–1073.
8 D. S. Tyler, J. Vappiani, T. Cañeque, E. Y. Lam, A. Ward, O. Gilan, Y.-C. Chan, A. Hienzsch, A. Rutkowska, T. Werner, A. J. Wagner, D. Lugo, R. Gregory, C. R. Molina, N. Garton, C. R. Wellaway, S. Jackson, L. MacPherson, M. Figueiredo, S. Stolzenburg, C. C. Bell, C. House, S.-J. Dawson, E. D. Hawkins, G. Drewes, R. K. Prinjha, R. Rodriguez, P. Grandi and M. A. Dawson, *Science*, 2017, **356**, 1397–1401.
9 K. A. Menear, C. Adcock, R. Boulter, X.-l Cockcroft, L. Copsey, A. Cranston, K. J. Dillon, J. Drzewiecki, S. Garman, S. Gomez, H. Javaid, F. Kerrigan, C. Knights, A. Lau, V. M. Loh, I. T. W. Matthews, S. Moore, M. J. O'Connor, G. C. M. Smith and N. M. B. Martin, *J. Med. Chem.*, 2008, **51**, 6581–6591.
10 A. Rutkowska, D. W. Thomson, J. Vappiani, T. Werner, K. M. Mueller, L. Dittus, J. Krause, M. Muelbaier, G. Bergamini and M. Bantscheff, *ACS Chem. Biol.*, 2016, **11**, 2541–2550.
11 M. Di Antonio, G. Biffi, A. Mariani, E.-A. Raiber, R. Rodriguez and S. Balasubramanian, *Angew. Chem., Int. Ed.*, 2012, **51**, 11073–11078.
12 R. Chaudhuri, T. Prasanth and J. Dash, *Angew. Chem., Int. Ed.*, 2023, **62**, e202215245.
13 P. Saha, D. Panda and J. Dash, *Chem. Commun.*, 2019, **55**, 731–750.
14 R. Rodriguez, S. Mueller, J. A. Yeoman, C. Trentesaux, J.-F. Riou and S. Balasubramanian, *J. Am. Chem. Soc.*, 2008, **130**, 15758.
15 R. Rodriguez, K. M. Miller, J. V. Forment, C. R. Bradshaw, M. Nikan, S. Britton, T. Oelschlaegel, B. Xhemalce, S. Balasubramanian and S. P. Jackson, *Nat. Chem. Biol.*, 2012, **8**, 301–310.
16 A. De Cian, E. DeLemos, J.-L. Mergny, M.-P. Teulade-Fichou and D. Monchaud, *J. Am. Chem. Soc.*, 2007, **129**, 1856–1857.
17 J. Lefebvre, C. Guetta, F. Poyer, F. Mahuteau-Betzer and M. P. Teulade-Fichou, *Angew. Chem., Int. Ed.*, 2017, **56**, 11365–11369.
18 M. Tera, H. Ishizuka, M. Takagi, M. Suganuma, K. Shin-ya and K. Nagasawa, *Angew. Chem., Int. Ed.*, 2008, **47**, 5557–5560.
19 M. Yasuda, Y. Ma, S. Okabe, Y. Wakabayashi, D. Su, Y.-T. Chang, H. Seimiya, M. Tera and K. Nagasawa, *Chem. Commun.*, 2020, **56**, 12905–12908.
20 H. Su, J. Xu, Y. Chen, Q. Wang, Z. Lu, Y. Chen, K. Chen, S. Han, Z. Fang, P. Wang, B.-F. Yuan and X. Zhou, *J. Am. Chem. Soc.*, 2021, **143**, 1917–1923.
21 X. Zhang, J. Spiegel, S. Martínez Cuesta, S. Adhikari and S. Balasubramanian, *Nat. Chem.*, 2021, **13**, 626–633.
22 S. Y. Yang, P. Lejault, S. Chevrier, R. Boidot, A. G. Robertson, J. M. Wong and D. Monchaud, *Nat. Commun.*, 2018, **9**, 4730.
23 I. Renard, M. Grandmougin, A. Roux, S. Y. Yang, P. Lejault, M. Pirrotta, J. M. Y. Wong and D. Monchaud, *Nucleic Acids Res.*, 2019, **47**, 5502–5510.
24 F. Rota Sperti, T. Charbonnier, P. Lejault, J. Zell, C. Bernhard, I. E. Valverde and D. Monchaud, *ACS Chem. Biol.*, 2021, **16**, 905–914.
25 F. Rota Sperti, B. Dupouy, J. Mitteaux, A. Pipier, M. Pirrotta, N. Chéron, I. E. Valverde and D. Monchaud, *JACS Au*, 2022, **2**, 1588–1595.
26 S. Y. Yang, D. Monchaud and J. M. Y. Wong, *Nat. Protoc.*, 2022, **17**, 870–889.
27 L. Stefan and D. Monchaud, *Nat. Rev. Chem.*, 2019, **3**, 650–668.
28 D. Monchaud, *Acc. Chem. Res.*, 2023, **56**, 350–362.
29 D. Monchaud, I. E. Valverde, P. Lejault and F. Rota Sperti, EP3889155A1, 2021; WO2021198239A1, 2021; US20230135545A1, 2023.
30 J. M. Baskin, J. A. Prescher, S. T. Laughlin, N. J. Agard, P. V. Chang, I. A. Miller, A. Lo, J. A. Codelli and C. R. Bertozzi, *Proc. Natl. Acad. Sci. U. S. A.*, 2007, **104**, 16793–16797.
31 Y. Rousselin, N. Sok, F. Boschetti, R. Guilard and F. Denat, *Eur. J. Org. Chem.*, 2010, 1688–1693.
32 R. Haudecoeur, L. Stefan, F. Denat and D. Monchaud, *J. Am. Chem. Soc.*, 2013, **135**, 550–553.
33 A. De Rache and J.-L. Mergny, *Biochimie*, 2015, **115**, 194–202.
34 A. T. Phan, V. Kuryavyi, S. Burge, S. Neidle and D. J. Patel, *J. Am. Chem. Soc.*, 2007, **129**, 4386–4392.
35 D. D. Le, M. Di Antonio, L. K. M. Chan and S. Balasubramanian, *Chem. Commun.*, 2015, **51**, 8048–8050.
36 S. Knör, A. Modlinger, T. Poethko, M. Schottelius, H. J. Wester and H. Kessler, *Chem. – Eur. J.*, 2007, **13**, 6082–6090.

37 J. Jamroskovic, I. Obi, A. Movahedi, K. Chand, E. Chorell and N. Sabouri, *DNA Repair*, 2019, **82**, 102678.
38 J. Mitteaux, P. Lejault, F. Wojciechowski, A. Joubert, J. Boudon, N. Desbois, C. P. Gros, R. H. E. Hudson, J.-B. Boulé, A. Granzhan and D. Monchaud, *J. Am. Chem. Soc.*, 2021, **143**, 12567–12577.
39 A. Laguerre, K. Hukezalie, P. Winckler, F. Katranji, G. Chanteloup, M. Pirrotta, J.-M. Perrier-Cornet, J. M. Wong and D. Monchaud, *J. Am. Chem. Soc.*, 2015, **137**, 8521–8525.
40 A. Laguerre, J. M. Y. Wong and D. Monchaud, *Sci. Rep.*, 2016, **6**, 32141.
41 S. Neidle, *J. Med. Chem.*, 2016, **59**, 5987–6011.
42 P. Lejault, J. Mitteaux, F. Rota Sperti and D. Monchaud, *Cell Chem. Biol.*, 2021, **28**, 436–455.
43 P. Thirumurugan, D. Matosiuk and K. Jozwiak, *Chem. Rev.*, 2013, **113**, 4905–4979.
44 J. E. Moses and A. D. Moorhouse, *Chem. Soc. Rev.*, 2007, **36**, 1249–1262.
45 Y. Feng, Z. He, Z. Luo, F. Rota Sperti, I. E. Valverde, W. Zhang and D. Monchaud, *iScience*, 2023, **26**, 106846.
46 V. S. Chambers, G. Marsico, J. M. Boutell, M. Di Antonio, G. P. Smith and S. Balasubramanian, *Nat. Biotechnol.*, 2015, **33**, 877–881.
47 R. Hänsel-Hertsch, D. Beraldi, S. V. Lensing, G. Marsico, K. Zyner, A. Parry, M. Di Antonio, J. Pike, H. Kimura and M. Narita, *Nat. Genet.*, 2016, **48**, 1267–1272.
48 Y. Feng, S. Tao, P. Zhang, F. Rota Sperti, G. Liu, X. Cheng, T. Zhang, H. Yu, X.-E. Wang, C. Chen, D. Monchaud and W. Zhang, *Plant Physiol.*, 2022, **188**, 1632–1648.
49 K.-w Zheng, J.-y Zhang, Y.-d He, J.-y Gong, C.-j Wen, J.-n Chen, Y.-h Hao, Y. Zhao and Z. Tan, *Nucleic Acids Res.*, 2020, **48**, 11706–11720.
50 W. W. I. Hui, A. Simeone, K. G. Zyner, D. Tannahill and S. Balasubramanian, *Sci. Rep.*, 2021, **11**, 23641.
51 J. Lyu, R. Shao, P. Y. Kwong Yung and S. J. Elsässer, *Nucleic Acids Res.*, 2021, **50**, e13.
52 G. Biffi, D. Tannahill, J. McCafferty and S. Balasubramanian, *Nat. Chem.*, 2013, **5**, 182–186.
53 S. Galli, L. Melidis, S. M. Flynn, D. Varshney, A. Simeone, J. Spiegel, S. K. Madden, D. Tannahill and S. Balasubramanian, *J. Am. Chem. Soc.*, 2022, **144**, 23096–23103.
54 C. K. Kwok, G. Marsico, A. B. Sahakyan, V. S. Chambers and S. Balasubramanian, *Nat. Methods*, 2016, **13**, 841–844.
55 J. Zhao, E. Y.-C. Chow, P. Y. Yeung, Q. C. Zhang, T.-F. Chan and C. K. Kwok, *BMC Biol.*, 2022, **20**, 257.
56 C. J. Maltby, J. P. R. Schofield, S. D. Houghton, I. O'Kelly, M. Vargas-Caballero, K. Deinhardt and M. J. Coldwell, *Nucleic Acids Res.*, 2020, **48**, 9822–9839.
57 A. A. Surani and C. Montiel-Duarte, *STAR Protoc.*, 2022, **3**, 101372.
58 A. De Magis, M. Kastl, P. Brossart, A. Heine and K. Paeschke, *BMC Biol.*, 2021, **19**, 45.